Heliyon 7 (2021) e08273

Contents lists available at ScienceDirect

Heliyon

journal homepage: www.cell.com/heliyon

Research article

Experimental study of the potential for thermal energy recovery with thermoelectric devices in low displacement diesel engines

R. Ramírez-Restrepo [a,b], A. Sagastume-Gutiérrez [b], J. Cabello-Eras [b], B. Hernández [a], J. Duarte-Forero [a,*]

[a] KAI Research Unit, Department of Mechanical Engineering, Universidad del Atlántico, Carrera 30 Número 8–49, Puerto Colombia, Barranquilla, Colombia
[b] Department of Energy, Universidad de la Costa CUC, Calle 58 Número 55 - 66, Barranquilla, Colombia

ARTICLE INFO

Keywords:
Energy efficiency
Internal combustion engine
Thermoelectric generator
Thermoelectric module

ABSTRACT

Improving the thermal efficiency of internal combustion engines is essential to reduce the operating costs and complaints with the increasing environmental requirements. Thermoelectric generators came up as an opportunity to reuse part of the heat loss with the exhausts. This paper evaluates the performance of a thermoelectric generator to improve the efficiency of a stationary diesel engine under different rotational speeds and torques. The data was obtained through CFD simulations and validated with experiments. The proposed solution uses a cooling system to control the temperature of the thermoelectric modules. The results show that the torque and the rotational speed of the engine are the most significant performance parameters of the thermoelectric generator, while the influence of the cooling water temperature has a minor but still significant influence. Additionally, the results show a change from 1.3% to 6.2% in the thermoelectric generator efficiency, while the exergy efficiency varies between 1.8% and 7.9%. The exergy balance indicates that most of the exergy is loss because of the irreversibilities in the thermoelectric generator and of the exergy loss with the exhausts. The exergy loss can be reduced by optimizing the design of the heat exchanger. Since the thermoelectric generator improved the engine efficiency by a marginal 0.2%–0.8%. Therefore, it is important to further research how to improve the design of heat exchangers for thermoelectric generators to increase their energy conversion efficiency and their impact on the energy efficiency of internal combustion engines.

1. Introduction

Internal combustion engines (ICE) are widely used in multiple applications, including transport, agriculture activities, industry, and power generation [1, 2, 3, 4, 5]. However, the increased exploitation of ICEs is one main driver of the accelerated depletion of fossil fuels and the large emissions of greenhouse gases and other pollutants [6, 7, 8, 9]. Commercial vehicles represent around 38% of the global consumption of fossil fuels [10] while accounting for 16.4% of the global emissions of CO_2 [11,12].

From 20% to 40% of the chemical energy in the fuel is converted into useful power during the operation of ICEs (i.e., depending on the engine cycle - gasoline or diesel - and technology), while 5% is dissipated by the friction in the mechanical components, and the remaining energy is loss as heat [13]. Based on the significance of heat losses in ICEs, the development and implementation of alternatives for heat recovery is a crucial commitment to meet the environmental standards of efficiency and operation. Consequently, the development of systems for waste heat recovery (WHR) has been gradually increasing interest [15]. There are different WHR systems available to reduce fuel consumption in ICEs by up to 10% [14].

In Colombia, stationary diesel engines are used to support electric power generation in non-interconnected areas [16]. Stationary diesel engines operate at high compression rates with a rather stable load, resulting in high exhaust temperatures, making them ideal technologies for WHR applications [17]. The development of WHR technologies includes the Rankine cycle [18], the Kalina cycle [19], the Rankine organic cycle [20, 21, 22], and the use of thermoelectric modules (TEM) [23]. Particularly, TEMs convert heat into electricity in the presence of a temperature gradient, based on the Seebeck effect [24, 25]. Additionally, TEMs include some advantages like the absence of moving parts, a compact structure, scalability, negligible maintenance costs, zero emissions, quiet operation, and high reliability [26]. Thermoelectric

* Corresponding author.
E-mail address: jorgeduarte@mail.uniatlantico.edu.co (J. Duarte-Forero).

https://doi.org/10.1016/j.heliyon.2021.e08273
Received 22 May 2021; Received in revised form 5 August 2021; Accepted 25 October 2021

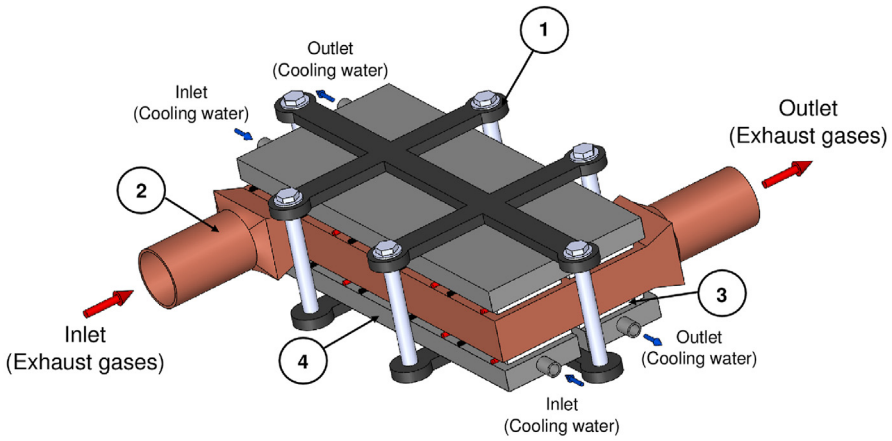

1. Support structure, 2. Heat exchanger, 3. Thermoelectric module (TEM), 4. Rectangular duct

a) Thermoelectric generator

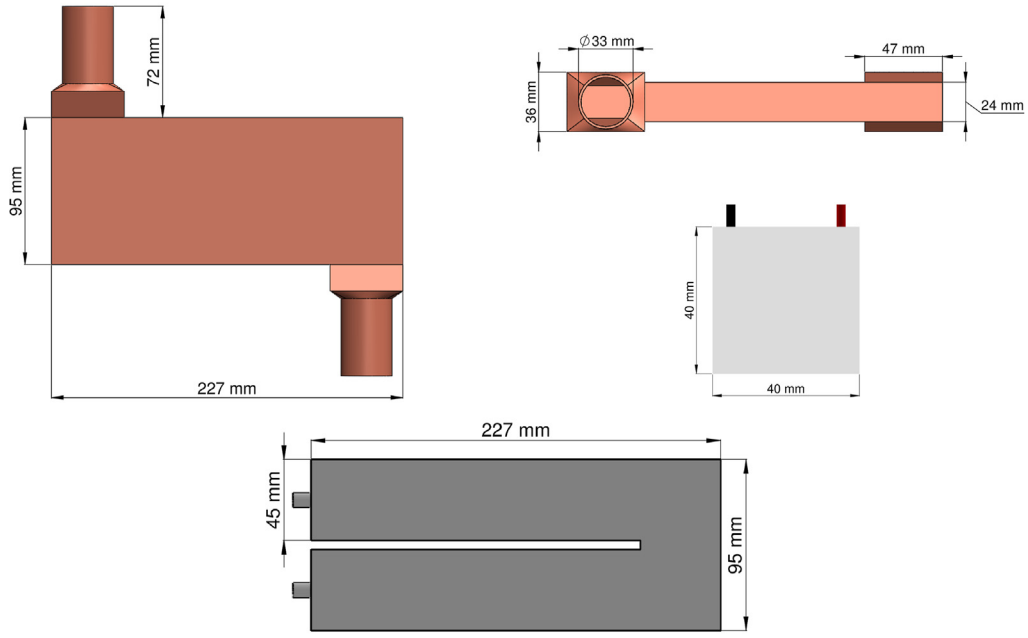

b) Dimension of TEG components

Figure 1. Thermoelectric generator.

generators (TEG) integrate TEMs with a heat exchanger and a cooling system in [26].

Recently, several studies focused on the heat recovery potential of TEGs implemented in commercial and heavy-duty vehicles [27, 28, 29]. Studies discussing the application of TEGs focus on the influence of operational variables like the temperature of the surface s and the pressure drop, other aspects like the heat exchanger materials, or the characteristics of TEMs, on the overall conversion efficiency of TEGs [30, 31]. Accordingly, Liu et al. [32] discussed the flow distribution effects on temperature gradient and performance metrics of the heat exchanger. Moreover, Marvao et al. [33] compared the influence of fin thickness, height, and spacing characteristics for three different fin-type heat exchangers on the overall performance of TEGs. Similarly, Lu et al. [34] assessed the effect of different types of metallic foam used for heat exchangers on the pressure drop and energy conversion performance of a TEG. Likewise, Rezania et al. [35] studied the influence of the cooling flow and the turbulent interactions on the temperature distribution of TEMs, while Karri et al. [36] assessed different cooling flow rates to maximize the energy conversion in TEGs. On the other hand, Li et al. [37] performed an energy and exergy analysis of a hybrid photovoltaic-thermoelectric system, showing that a high concentration ratio combined with thermoelectric modules leads to higher efficiencies. Makki et al. [38] investigated a photovoltaic - thermoelectric generator using heat pipes aided by numerical models, evidencing that integrating TEGs with photovoltaic units can take advantage of the waste heat of the system, increasing the electric conversion efficiency.

Regardless of the extensive discussion addressing the integration of TEG into vehicles, most studies consider stationary operating conditions. These conditions are far from the real operating conditions in vehicles and represent an important limitation to estimate the energy recovery potential of TEGs accurately [33, 39, 40, 41, 42]. Engine load directly defines the composition, properties, flow, and temperature of the

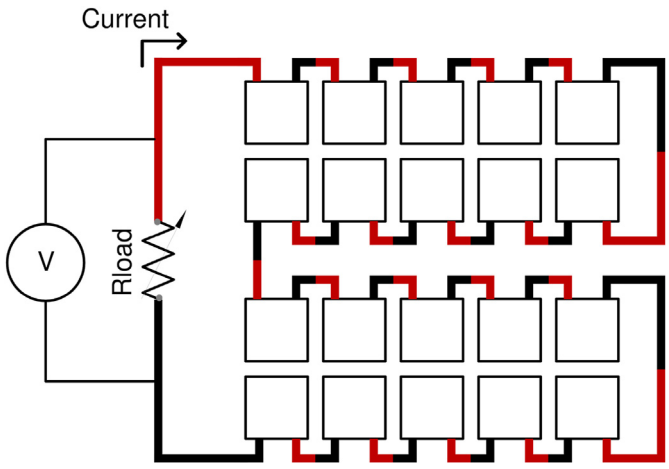

Figure 2. Electric configuration of thermoelectric modules.

exhaust, which influences the overall performance of TEGs [43, 44, 45]. Other aspects like the mitigation of polluting emissions and the influence on the fuel economy of the engine, which can stress the benefits of TEGs, are frequently excluded from studies.

To overcome the limitation of previous studies, the present study aims at characterizing the energy recovery potential of a TEG integrated into a low displacement diesel engine. To this end, the energy and exergy balances will be used. Additionally, an environmental and economic analysis will be developed to further highlight the performance of the TEG and its influence on the engine. To this end, experimental and simulated data of the TEG performance under different conditions will be used. Therefore, this paper contributes to characterizing the energy conversion efficiency of TEGs under different operating conditions as an energy recovery alternative in diesel engines. In what follows, Section 2 describes the methodology used in the study, the characteristics of the test bench, and the formulation of the energy analysis. Section 3 outlines the core findings and critically discusses the results. Finally, Section 4 provides the concluding remarks, limitations, and future perspectives.

2. Materials and methods

An experimental test bench was built, which includes a stationary diesel engine, a TEG, and a data acquisition (DAQ) system, which is described in this section.

2.1. Experimental setup

Figure 1 shows the drawings of the thermoelectric generator used during the experimental tests developed in this study.

The TEG includes a heat exchanger, a cooling system, 20 TEMs (model TEG1-12610-5.1), and a supporting structure. The TEMs are symmetrically distributed on both sides of the heat exchanger, with 10 TEMs on the upper surface and 10 on the lower surface. A thin layer of thermal putty was applied between TEMs and the hot and cold surfaces to improve the heat transfer. This reduces the air between the surface and TEMs, compensating for the surface irregularities. The number of TEMs used in the TEG was defined based on the available surface on the heat exchanger. The cooling ducts, located on the cold surface of TEMs, are used to control the temperature in this surface during the experiments, to define the impact of ambient temperature on the TEG performance. The cooling system circulates water that is cooled to a defined temperature in a chiller.

Figure 2 shows the electric configuration of the TEG.

In this case, TEMs are connected in series to a variable resistance (Rload) that is used to define the energy recovery potential of the TEG at different engine loads. Notice that the selection of the TEG array (series) is supported by the temperature gradient on the surface of the heat exchanger (i.e., the temperature variation of the surface between the inlet and the outlet of the TEG), which affects the electric efficiency of the TEMs.

The series arrangement was selected based on the fact that it yields higher efficiencies than the parallel arrangement, as demonstrated by Montecucco et al. [46]. This is explained by the lower voltage and higher current levels resulting in electric losses because of the Joule heating phenomena. The variable resistance adjusts the electric load according to the TEG performance (i.e., when the TEG reaches its maximum electric power generation capacity, the external resistance equals the resistance of the circuit of TEMs).

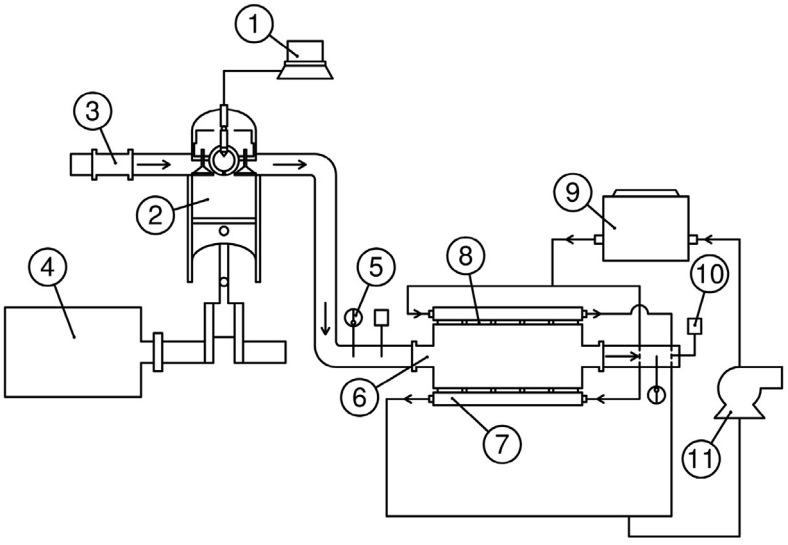

1. Gravimetric flow meter, 2. Diesel engine, 3. Airflow meter, 4. Dynamometer, 5. Temperature sensor, 6. Heat exchanger, 7. Rectangular duct, 8. Thermoelectric module, 9. Chiller, 10. Pressure sensor, 11. Water pump.

Figure 3. Experimental test bench.

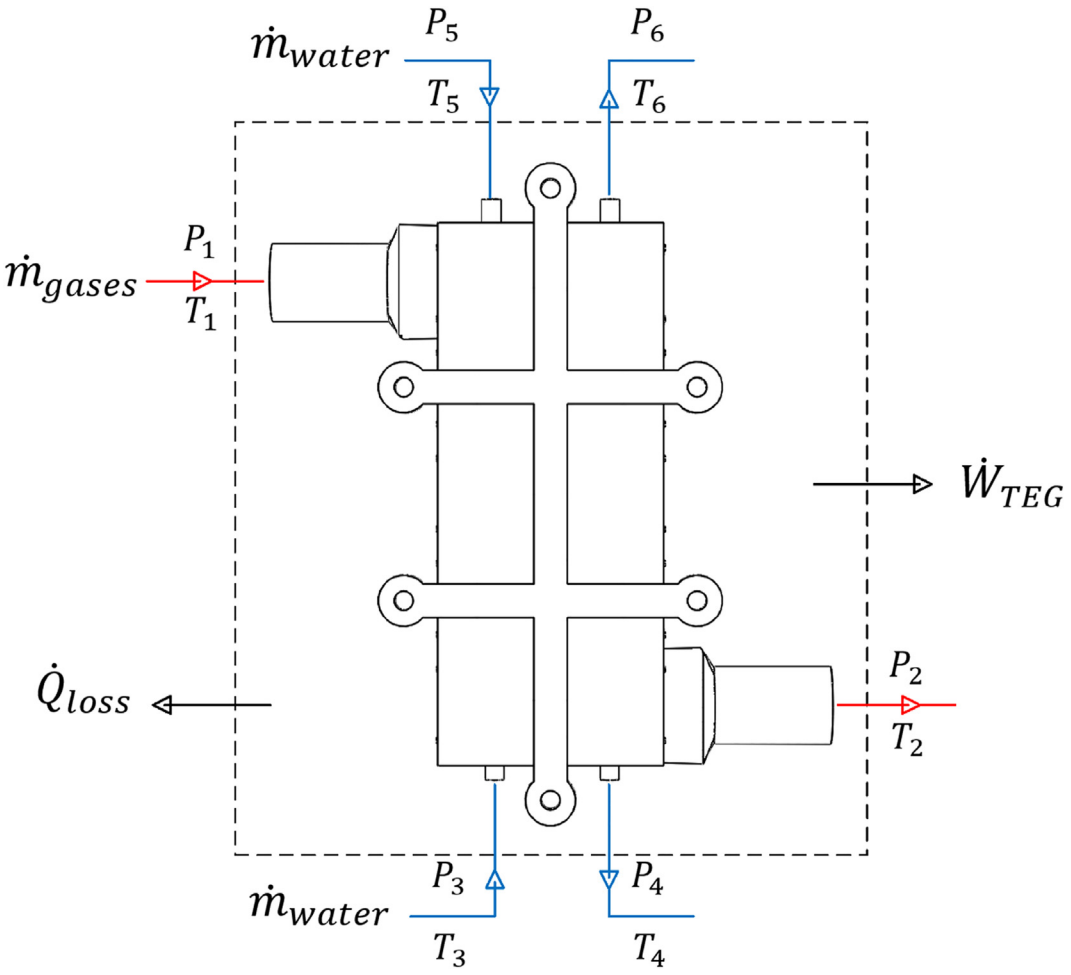

Figure 4. Energy flows in the TEG.

Based on the characteristics of the ICE, the backpressure introduced with the TEG on the exhausts must be under 2 kPa to prevent negative impacts on the energy efficiency of the engine (i.e., that the efficiency loss resulting from the backpressure surpass the efficiency gains obtained with the TEG). The latter is an important constraint in the design of TEGs to guarantee the adequate functionality of ICEs. Therefore, the heat exchanger must ensure the highest possible heat exchange rate without exceeding the pressure drop limit defined by the engine backpressure limit. A CFD simulation was implemented using OpenFOAM® to ensure the highest heat transfer rate in the heat exchanger while limiting the backpressure under 2.00 kPa. Results from the simulation show that the highest pressure drop resulting from the TEG was 1.20 kPa, which is lower than the 2.00 kPa admissible by the engine. Therefore, this design guarantees the normal operation of the engine.

Figure 3 displays a schematic representation of the complete engine test bench.

The instrumentation of the test bench is essential for data acquisition and monitoring. For this experiment, the temperatures at the input and output of the heat exchanger were measured with K-type thermocouples. Moreover, the pressures at the input and output of the TEG were measured using piezoresistive pressure sensors (model PSA-C01). Fuel consumption was measured with a gravimetric flow meter, while the combustion airflow was registered with an airflow meter (model 22680 -7J600). The cooling water temperature was controlled with a chiller and a water pump that maintained a water flow rate of 6 L/min, keeping the cooling water temperature constant.

2.2. Energy analysis

Energy and exergy balances were used to assess the performance of the TEG.

2.2.1. Energy balance of the TEG

Figure 4 illustrates the input and output energy flows in the TEG system.

A flow of energy inputs the TEG with the gas flow through the heat exchanger, where part of the heat transferred is converted into electricity in the TEMs, while some heat is loss to the cooling water flow, and some heat is dissipated to the environment. The energy balance can be described by Eqs. (1), (2), and (3).

$$\dot{Q}_{TEG} = \dot{W}_{TEG} + \dot{Q}_{water} + \dot{Q}_{loss} \tag{1}$$

$$\dot{Q}_{TEG} = \dot{m}_{gases} \cdot C_{p,gases}\left[T_{(1)} - T_{(2)}\right] \tag{2}$$

$$\dot{Q}_{water} = \dot{m}_{water} \cdot C_{p,water} \cdot \left[T_{(4)} - T_{(3)}\right] + \dot{m}_{water} \cdot C_{p,water} \cdot \left[T_{(6)} - T_{(5)}\right] \tag{3}$$

where $\dot{Q}$, $\dot{W}_{TEG}$, T, $\dot{m}$ and C_p are the heat flow, electrical power generated by the TEG, temperature, mass flow rate, and specific heat, respectively.

Since the equivalence ratio in diesel engines is less than one, the combustion gases can be considered as an ideal gas [47]. Therefore, the C_p of the exhaust gases are calculated as a function of temperature of the gas flow like [48]:

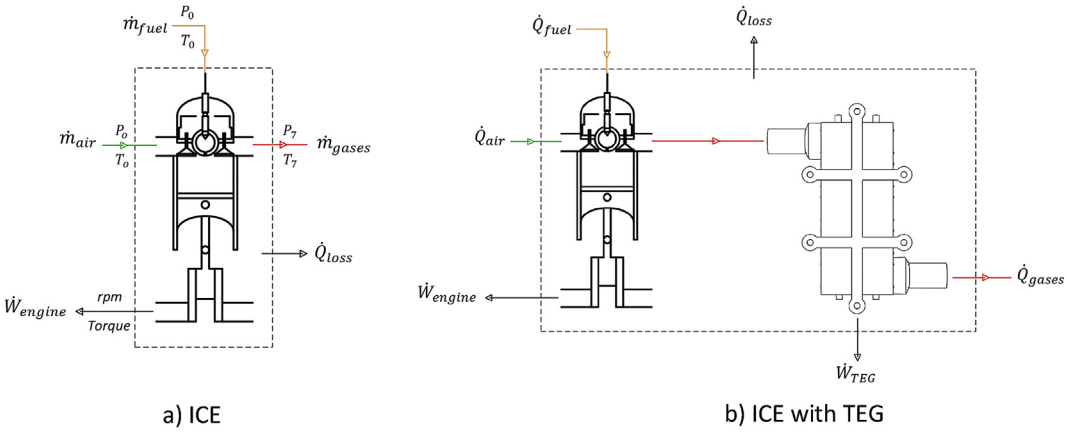

Figure 5. Energy flow diagram in ICEs.

$$C_{p,gases} = 28.11 + 0.1967 \times 10^{-2}T + 0.4802 \times 10^{-5}T^2 - 1.966 \times 10^{-9}T^3 \tag{4}$$

Moreover, the energy efficiency of the TEG (η_{TEG}) is defined as the ratio between the generated electric power and the heat transfer rate in the heat exchanger, as following

$$\eta_{TEG} = \frac{\dot{W}_{TEG}}{\dot{Q}_{TEG}} \tag{5}$$

2.2.2. Exergy balance of the TEG

The exergetic analysis was developed calculating the entropy generation (S_{TEG}) and the exergy efficiency ($\eta_{exer,TEG}$), which were defined as:

$$S_{TEG} = \frac{\dot{E}_{d,TEG}}{T_o} = \frac{\dot{m}_{gases} \cdot (e_1 - e_2) - \dot{W}_{TEG}}{T_o} \tag{6}$$

$$\eta_{exer,TEG} = \frac{\dot{W}_{TEG}}{\dot{E}_{\dot{m},gases(1)}} \tag{7}$$

where $\dot{E}_{\dot{m},gases(1)}$ and e is the exergy and e_i the specific exergy of the input and output exhaust flow, respectively.

The parameters required for Eq. (7) were calculated like:

$$\dot{E}_{\dot{m},gases(1)} = (\dot{m}_{air} + \dot{m}_{fuel}) \cdot \left(C_{p,gases} \cdot (T_{(1)} - T_o) - T_o \cdot \left[C_{p,gases} \cdot ln\left(\frac{T_1}{T_o}\right) - R \cdot ln\left(\frac{P_1}{P_o}\right)\right]\right) \tag{8}$$

$$e_1 = C_{p,gases} \cdot (T_{(1)} - T_o) - T_o \cdot \left[C_{p,gases} \cdot ln\left(\frac{T_1}{T_o}\right) - R \cdot ln\left(\frac{P_1}{P_o}\right)\right] \tag{9}$$

$$e_2 = C_{p,gases} \cdot (T_{(2)} - T_o) - T_o \cdot \left[C_{p,gases} \cdot ln\left(\frac{T_2}{T_o}\right) - R \cdot ln\left(\frac{P_2}{P_o}\right)\right] \tag{10}$$

where T_o and P_o are the reference environmental temperature and pressure, defined at 28 °C and 1 atm, respectively.

2.2.3. Energy balance of the engine

In practice, ICEs aim at converting the highest amount of the chemical energy of fuels into mechanical power.

After fuel combustion, a fraction of the energy released is transformed into mechanic power, while a significant share is loss through friction to the refrigeration system and with the exhausts (see Figure 5a). Using a TEG is possible to recover a fraction of the energy loss with the exhaust (see Figure 5b).

The energy balance of the engine-TEG system is calculated as shown in Eq. (11).

$$\dot{Q}_{fuel} + \dot{Q}_{air} = \dot{W}_{engine} + \dot{W}_{TEG} + \dot{Q}_{loss} + \dot{Q}_{gases} \tag{11}$$

where $\dot{Q}_{fuel}$ represents the energy of the fuel and $\dot{Q}_{loss}$ account for energy loss in the engine and the TEG.

The energy of the fuel was calculated as a relation between the flow of fuel and its heating value (LHV), defined as 44.05 MJ/kg in this case [12]:

$$\dot{Q}_{fuel} = \dot{m}_{fuel} \cdot LHV \tag{12}$$

The output power ($\dot{W}_{engine}$) of the engine was calculated as a function of the torque (T_r) and of the engine rotation speed (N) like:

$$\dot{W}_{engine} = 2\pi \cdot N \cdot T_r \tag{13}$$

The loss with the exhausts at the engine output ($\dot{Q}_{gases}$) was calculated as:

$$\dot{Q}_{gases} = (\dot{m}_{fuel} + \dot{m}_{air}) \cdot C_{p,gases} \cdot T_{(2)} \tag{14}$$

The energy efficiency for the ICE without TEG was calculated as follows.

$$\eta_{engine} = \frac{\dot{W}_{engine}}{\dot{m}_{fuel} \cdot LHV + \dot{Q}_{air}} \tag{15}$$

Moreover, the energy efficiency for the ICE with TEG is calculated as:

$$\eta_{engine+TEG} = \frac{\dot{W}_{engine} + \dot{W}_{TEG}}{\dot{m}_{fuel} \cdot LHV + \dot{Q}_{air}} \tag{16}$$

2.2.4. Exergy balance of the engine

The exergy balance for the engine-TEG system was calculated as the sum of the exergies... as shown in Eq. (17)

$$\dot{E}_{fuel} = \dot{E}_{\dot{W},engine} + \dot{E}_{\dot{W},TEG} + \dot{E}_{loss} + \dot{E}_{gases} + \dot{E}_{dest} \tag{17}$$

where $\dot{E}_{fuel}, \dot{E}_{\dot{W},engine}, \dot{E}_{\dot{W},TEG}, \dot{E}_{loss}, \dot{E}_{gases}$ and $\dot{E}_{dest}$ are the exergy of the injected fuel, the work carried out by the engine, the work generated by the TEG, the loss exergy, the exergy of the gases expelled into the atmosphere, and the destruction of exergy, respectively.

The exergy of the fuel ($\dot{E}_{fuel}$)is calculated like:

$$\dot{E}_{fuel} = \dot{m}_{fuel} \cdot LHV \cdot \varphi \tag{18}$$

where φ is the chemical exergy factor of the fuel. A chemical exergy factor of 1.072 is defined for commercial diesel [49].

The exhaust exergy ($\dot{E}_{gases}$) and exergy loss ($\dot{E}_{loss}$) were calculated using Eqs. (19) and (20), respectively:

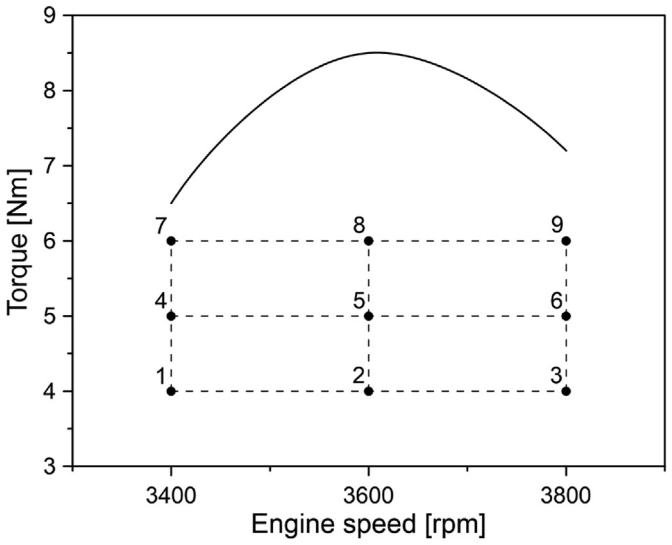

Figure 6. Engine operating conditions.

Table 1. Physicochemical properties of commercial diesel [12].

Property	Units	Value	Standard
Cloud point	°C	6.5	ASTM D2500
Flashpoint	°C	76.0	ASTM D93
Density	kg/m^3	821.5	ASTM D1298
Pour point	°C	3.1	ASTM D97
Viscosity	cSt	2.64	ASTM D445
LHV	MJ/kg	44.05	ASTM D240

$$\dot{E}_{gases} = \left(\dot{m}_{air} + \dot{m}_{fuel}\right) \cdot \left[C_{p,gases} \cdot (T_2 - T_o) - T_o \cdot \left(C_{p,gases} \cdot ln\left(\frac{T_2}{T_o}\right) - R \cdot ln\left(\frac{P_2}{P_o}\right)\right)\right] \quad (19)$$

$$\dot{E}_{loss} = \dot{Q}_{loss}\left(1 - \frac{T_o}{T_s}\right) \quad (20)$$

where T_o and T_s are the ambient temperature and the average surface temperature of the engine, respectively. The calculation of the entropy generation $(S_{gen})$is developed as:

$$S_{gen} = \frac{\dot{E}_{dest}}{T_o} \quad (21)$$

The exergy efficiency of the engine $(\eta_{exer,engine})$ and the engine -TEG system $(\eta_{exer,engine+TEG})$ are calculated as:

$$\eta_{exer,engine} = \frac{\dot{E}_{product,engine}}{\dot{E}_{fuel}} = \frac{\dot{E}_{\dot{W},engine}}{\dot{E}_{fuel}} \quad (22)$$

$$\eta_{exer,engine+TEG} = \frac{\dot{E}_{product,engine+TEG}}{\dot{E}_{fuel}} = \frac{\dot{E}_{\dot{W},engine} + \dot{E}_{\dot{W},TEG}}{\dot{E}_{fuel}} \quad (23)$$

2.3. Experimental methodology

In total, nine operating points were selected for the experimental tests (see Figure 6).

The defined operating points defined consider three rotational speeds and three torques of the engine.

During the experiments, commercial diesel was used to fuel the engine. Table 1 shows the physicochemical properties of commercial diesel.

Table 2. Classification of the experimental test variables.

Classification	Operational variable	Unit	Nomenclature
Response variables	• Mechanical engine power	W	$\dot{W}_{engine}$
	• TEG electrical power	W	$\dot{W}_{TEG}$
	• Heat transferred to the walls of the exchanger	W	$\dot{Q}_{TEG}$
	• Exergy destruction rate	W	$\dot{E}_{d,TEG}$
Input variables	• Torque	Nm	T_r
	• Rotation speed	rpm	N
	• Cooling temperature	°C	T
Blocking and noise variables	• Fuel temperature	°C	T_{fuel}
	• Environmental temperature	°C	T_{amb}
	• Air temperature	°C	T_{air}
Uncontrolled variables	• Inlet pressure	kPa	P
	• Cylinder head temperature	°C	$T_{cylinder}$
	• Exhaust temperature	°C	T_{gases}

Table 3. Input variable levels.

Input variables	Units	Low	Medium	High
Torque	Nm	4	5	6
Rotation speed	rpm	3400	3600	3800
TEG water-cooling temperature	T	17	22	27

These values are the operating conditions considered during the experiments for the stationary engine.

Table 4. Engine operating conditions.

Operation mode	Torque (Nm)	Engine speed (rpm)	Output exhaust temperature (°C)	Exhaust flow (g/s)	Dosage (fuel/air)
1	4	3400	120	5.483	0.0371
2		3600	153	5.508	0.0382
3		3800	186	5.533	0.0394
4	5	3400	201	5.541	0.0403
5		3600	207	5.556	0.0402
6		3800	216	5.579	0.0426
7	6	3400	232	5.636	0.0434
8		3600	255	5.656	0.0436
9		3800	265	5.761	0.0439

To clearly define the effect of the different operating parameters affecting the engine performance, an experimental design was used to plan the experimental test. Consequently, the operational variables were classified into response, input, blocking, and noise variables (see Table 2).

Table 3 shows the three considered levels for the torque and rotation speed of the engine (i.e., low, medium, and high).

In this case, a multilevel factorial experimental design 3^2 was used for the input variables, which resulted in nine experiments. Table 4 depicts the operating conditions of the engine for the nine operating modes during the experiments.

To reduce the variability of the experimental results, each test was run three times. Thus, a total of 27 experimental runs were developed. To ensure steady-state operating conditions during the experimental tests, the system started measuring after the temperature of the exhausts remained constant during 30 s. Afterward, the DQA system measured for 5 min.

Figure 7 shows the energy efficiency of the engine for different operating conditions.

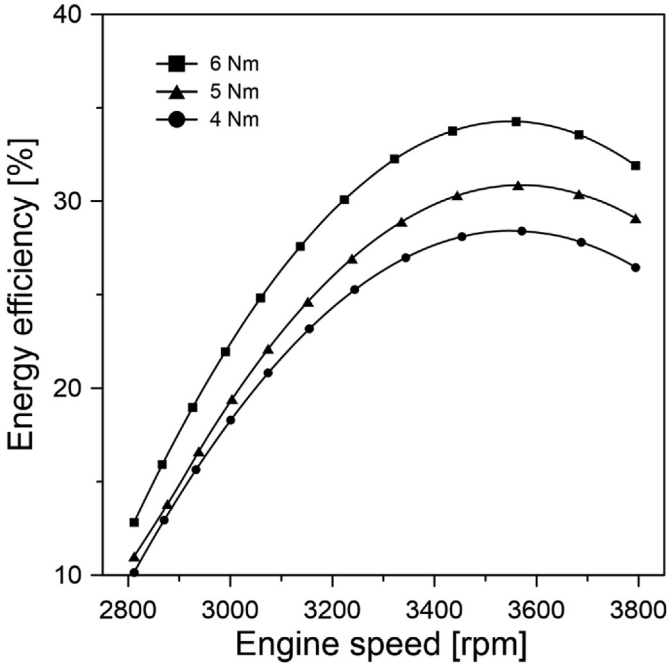

Figure 7. Efficiency of the engine under study.

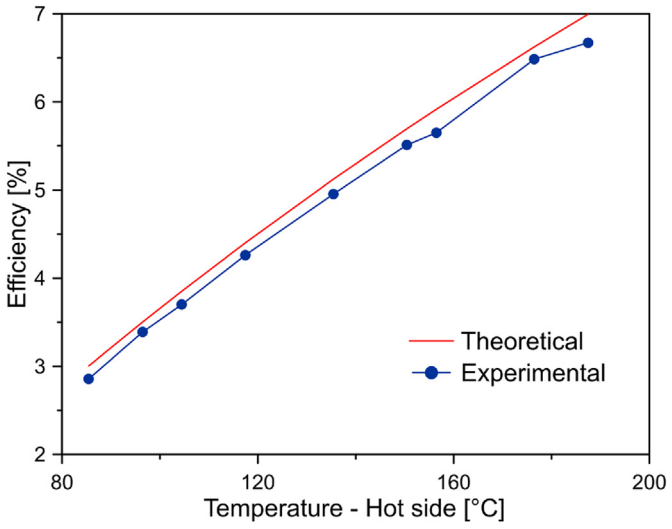

Figure 8. Energy conversion efficiency ($T_c = 27°C$).

The results show that the efficiency of the engine varies from 10% to 35% for the different operating conditions.

To evaluate the thermoelectric modules used in the experimental tests and evaluate their energy conversion efficiency, a comparative analysis of the conversion efficiency between the experimental (η_e) and ideal (η_t) performance was developed. The efficiencies were calculated as [50, 51]:

$$\eta_t = \left(\frac{T_h}{3.41 \cdot T_h + 2.41 \cdot T_c}\right) - \left(\frac{T_c}{3.41 \cdot T_h + 2.41 \cdot T_c}\right) \tag{24}$$

$$\eta_e = \frac{V^2}{R \cdot \dot{m}_g \cdot c_p \cdot \Delta T} \tag{25}$$

where T_h and T_c are the temperature of the hot and cold side of the TEM, V is the output voltage, R is the load resistance, $\dot{m}_g$ is the exhaust gas flow, c_p is the specific heat capacity and ΔT is the variation of the exhaust temperature.

Figure 8 shows the comparative analysis of the energy conversion efficiency of TEMs.

The figure shows that there is an agreement between the efficiency experimentally measured and theoretically calculated. Thus, the results ensure that the thermoelectric modules are in good technical conditions.

Figure 9 shows the characteristic curves of the thermoelectric modules.

3. Results

This section discusses the experimental results of the study.

3.1. Effect of the external resistance (R_{load})

Figure 10 shows the power generation in the TEG as a function of the electric resistance and operating conditions. The power generation reaches the highest output when the external electric resistance (R_{load}, see Figure 3) balances the sum of the TEMs electric resistances [52].

The results show that the power output in the TEG reaches a maximum at an average electric resistance of 60Ω. For lower or higher values, the power output reduces significantly. These results are in agreement with other investigations discussing the integration of TEG into commercial vehicles [42]. Furthermore, increasing the torque and the rotation speed results lead to a significant increase in the electric power output in the TEG. This is explained because increasing the torque and rotational speed results in the higher temperature of the surface in the hot side of the TEMs.

Table 5 shows the hot side temperature of the TEMs for different operating conditions of the considered engine.

These results are in agreement with other studies described in the specialized literature [53].

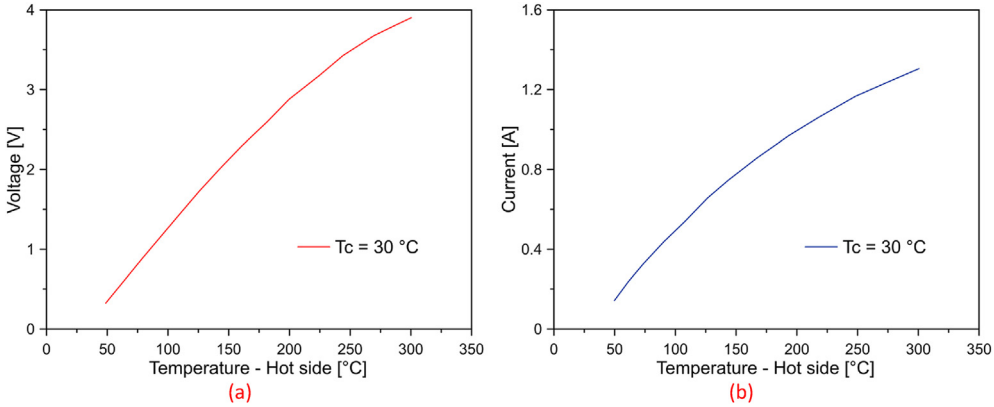

Figure 9. Curve of the thermoelectric module (a) voltage and (b) current.

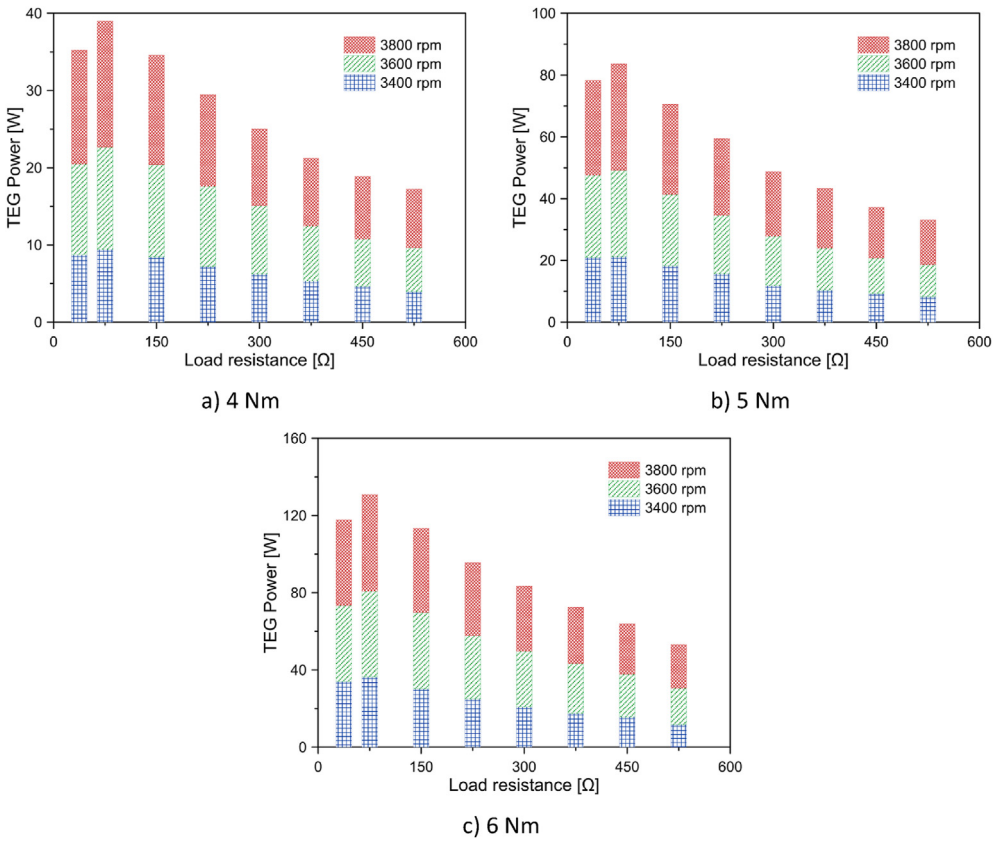

Figure 10. Power generation on the TEG.

Table 5. Hot side temperature of TEMs (°C).

TEM	Torque [Nm]			Torque [Nm]			Torque [Nm]		
	4			5			6		
	rpm			rpm			rpm		
	3400	3600	3800	3400	3600	3800	3400	3600	3800
1	85	96	104	117	135	150	156	176	187
2	86	97	105	118	136	151	157	177	188
3	85	96	104	117	135	150	156	176	187
4	83	94	102	115	133	148	154	174	185
5	81	92	100	113	131	146	152	172	183
6	86	97	105	118	136	151	157	177	188
7	86	97	105	118	136	151	157	177	188
8	86	97	105	118	136	151	157	177	188
9	83	94	102	115	133	148	154	174	185
10	83	94	102	115	133	148	154	174	185
11	87	98	106	116	137	149	155	175	186
12	89	99	104	120	135	150	155	175	186
13	88	98	105	118	133	152	154	174	185
14	82	93	103	117	134	150	152	172	183
15	78	90	99	114	129	145	153	173	184
16	85	96	107	116	138	153	155	175	186
17	85	95	106	120	134	149	155	175	186
18	87	98	103	116	137	152	158	178	189
19	85	96	100	113	131	149	153	173	184
20	82	92	104	116	135	150	156	176	187

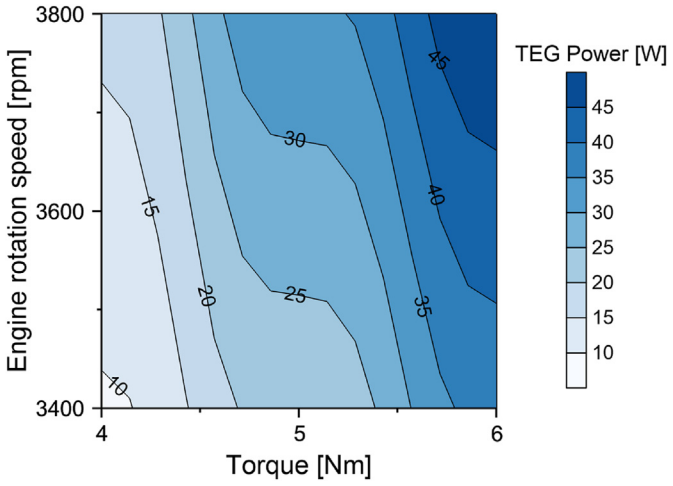

Figure 11. Electric power output in the TEG for a cooling water temperature of 27 °C.

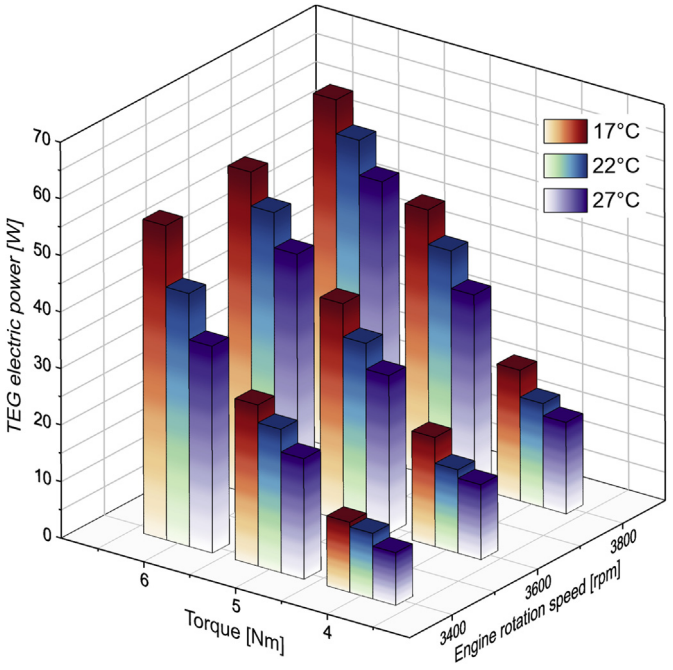

Figure 12. Electrical power for different TEG cooling water temperatures.

3.2. Engine torque effects

Figure 11 shows the electric power output from the TEG for the defined operating conditions.

The results show that the power output from the TEG increases with the increased engine torque for all the rotational speeds. Likewise, the power output from the TEG increases with the rotational speed for all the engine torques. This is explained because the higher flow of energy in the exhausts through the heat exchanger that results from the higher combustion temperatures supported by the increased fuel consumption with higher engine torques and rotational speeds [9].

In general, increasing the torque by 1 Nm doubles the output power in the TEG. Moreover, increasing the rotational speed of the engine by 200 rpm increases the power output in the TEG by 28%.

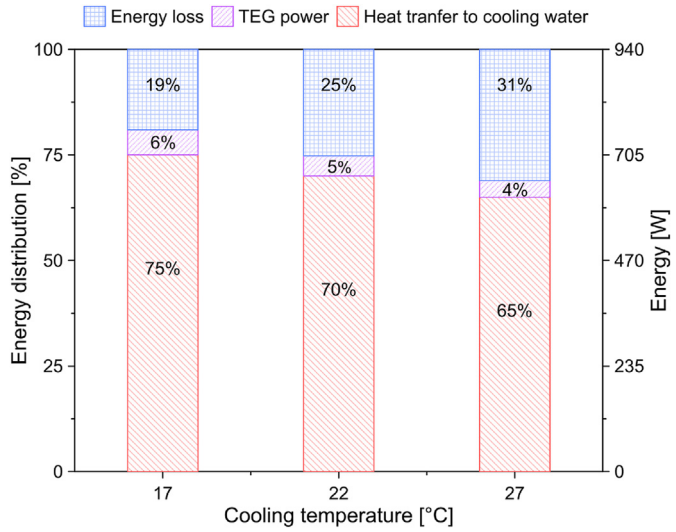

Figure 13. Energy balance of the TEG at 6 Nm and 3800 rpm.

3.3. TEG cooling water temperature effect

Figure 12 shows the variation of the electric power output in the TEG for the different cooling water temperatures considered in the experimental tests.

Results show that reducing the cooling water temperature increases the electric power output. Since the gradient of the temperature in the TEMs increases for lower cooling water temperatures. Thus, increasing the output voltage. Reducing the cooling water temperature by 5 °C increases the power output in the TEG by an average of 18%.

In ICEs, the loss with the gases varies from 30% to 35% of the energy input with the fuel. Friction losses account for some 5% of the fuel energy, while the cooling system accounts for 30%–40%, and the useful energy accounts for 25%–30%. A fraction of the heat loss can be recovered using TEGs to produce electricity. The use of DC-to-DC converters (power units) permits to matching of the output voltage of the TEG to the voltage required in the engine [54].

3.4. TEG energy analysis

Figure 13 shows the allocation of the energy balance in the TEG.

Results show that reducing the cooling water temperature increases the TEG power output while increasing the energy loss with the cooling water. In total, from 65% to 75% of the energy is loss to the cooling water, while 19–31% is dissipated as heat to the environment. In this case, 4%–6% of the energy is recovered into electric power.

The conversion efficiency of TEGs is usually less than 5%. The higher efficiency obtained in this study is mainly explained by the type of heat exchanger used in the TEG (see Figure 1). This heat exchanger has longer residence times of the exhaust ??, leading to higher heat exchange rates and higher surface temperatures on the hot side of TEMs. With this design, the TEMs recover more energy into electricity, which is an improvement contrasted to other heat exchanger geometries used in TEGs, as discussed in the specialized literature [53]. Furthermore, the efficiency values higher than 5% obtained for a cooling temperature of 17 °C on the cold surface of TEMs (see Figure 13) are explained by the higher temperature gradient in the TEMs that increases the conversion efficiency. Another significant factor is the technical characteristics of the TEMs used, which can operate under high temperatures (max. 300 °C).

Low conversion efficiencies in the TEG are a consequence of the low conversion efficiencies of TEMs because the current materials available have low conversion efficiencies, as well as because of negative physical phenomena such as the Thomson effect [26]. Therefore, the authors

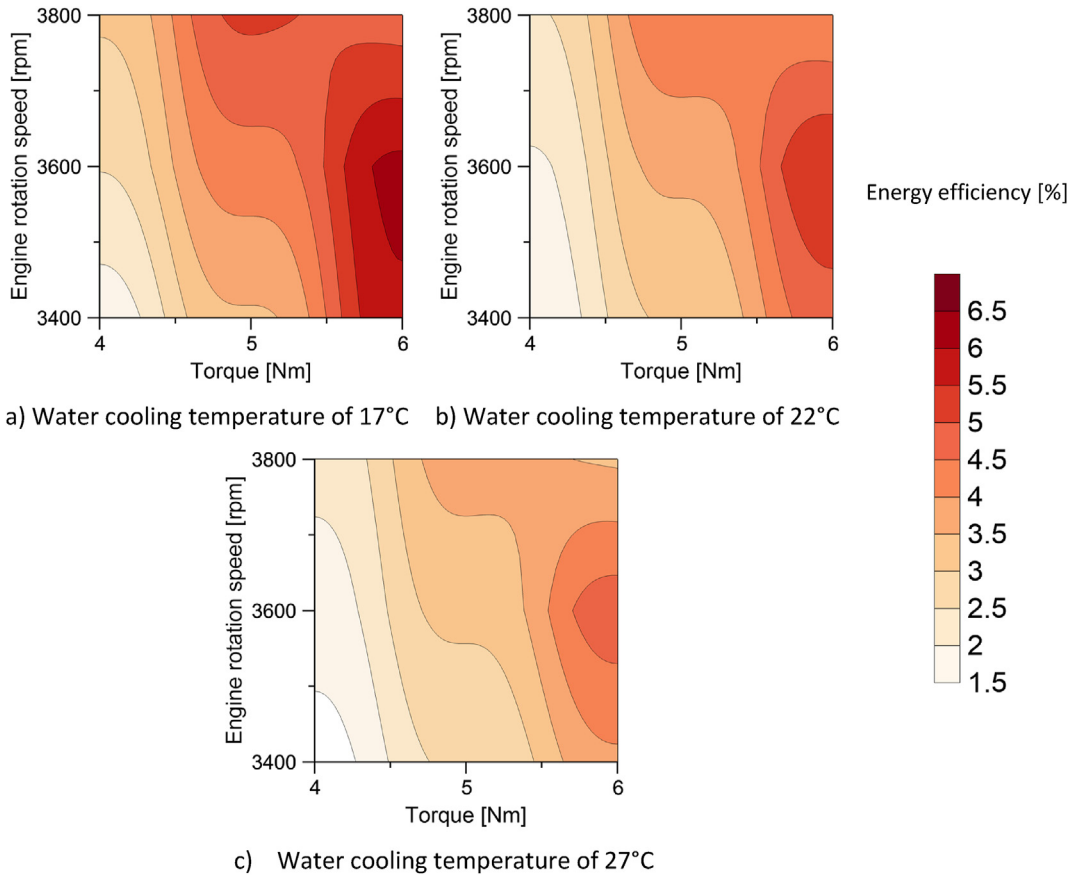

Figure 14. Energy conversion efficiency of the TEG for different operating conditions.

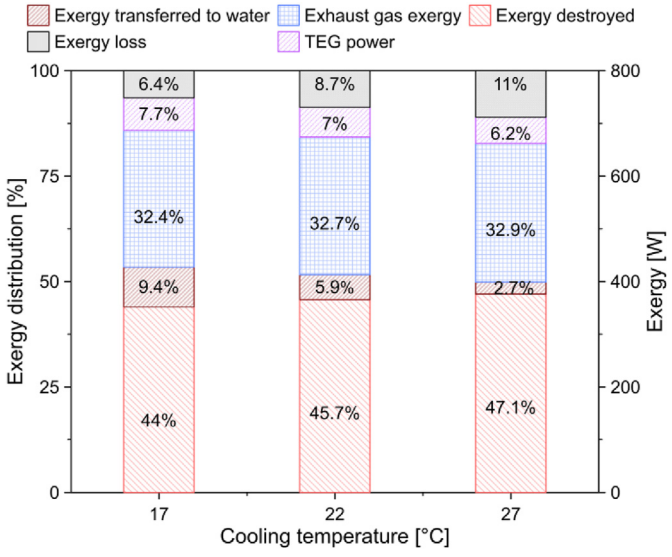

Figure 15. Exergy balance of the at 6 Nm and 3800 rpm.

considered that the development of new materials would help to increase the efficiency of these deceives.

Figure 14 illustrates the variation of the energy conversion efficiency in the TEG for different operating conditions.

Results show that the energy conversion efficiency of the TEG varies between 1.29% and 6.15%, increasing for lower values of the cooling water temperature for all the engine operating conditions, which is explained by an increment of the temperature gradient, as explained before (see Figure 12).

Regardless of the relatively low energy conversion efficiency, the adequate use of the electric power output from TEGs is a sound approach to reduce the fuel consumption of ICEs that leads to reduced airborne emissions [25]. Moreover, contrasted to WHR technologies like the ORC, the TEG has lower costs, and technological complexity requires less space and has higher reliability. These advantages can contribute to the widespread implementation of TEGs as a WHR alternative in vehicles.

3.5. TEG exergy analysis

Figure 15 shows the allocation of the exergy balance in the TEG.

Results show that reducing the cooling water temperature leads to higher electric power output, explained by the higher temperature gradient in the TEMs and the reduction of energy losses. In the process, the exergy loss with the exhausts and the exergy destruction account for most of the exergy input to the TEG (i.e., from 70% to over 80%). As compared to the energy balance, the exergy loss with the cooling water is little in the process. On average, increasing 5 °C in the cooling water temperature decreases exergy losses by 0.82%.

Figure 16 shows the variation of the exergy efficiency for different operational conditions.

Results show that reducing the cooling water temperature increases the exergy efficiency of the TEG for all the engine operating conditions. Like energy efficiency, increasing the engine torque and rotational speed also result in higher levels of exergy efficiency.

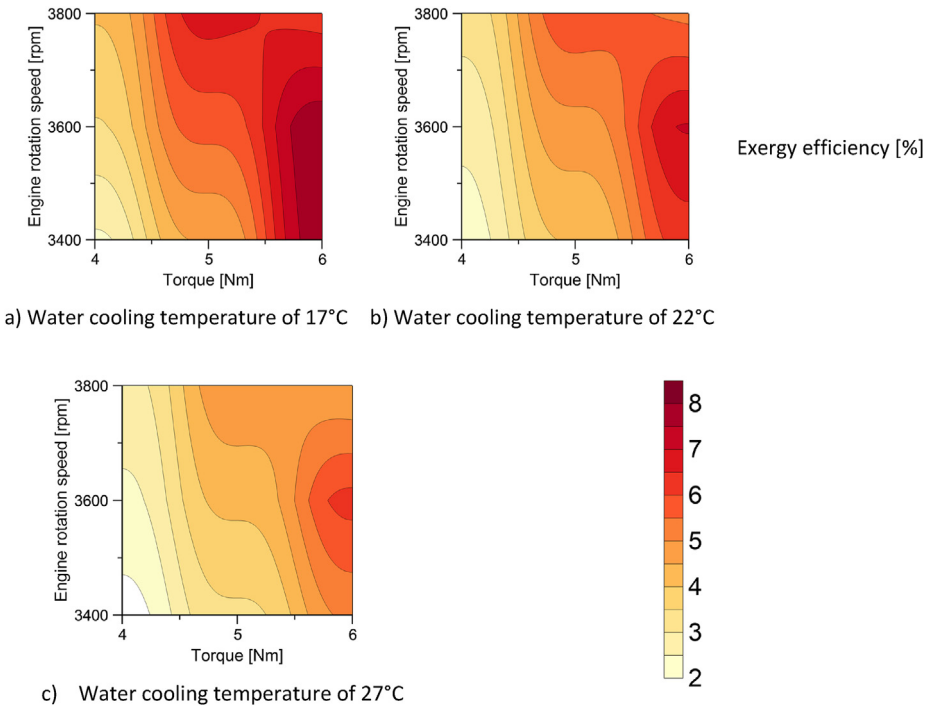

Figure 16. Exergy efficiency for different operating conditions.

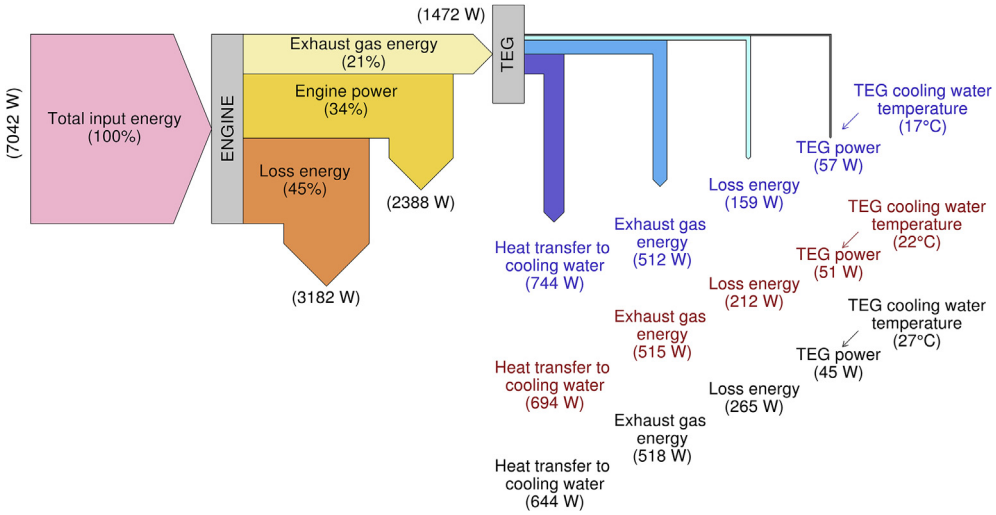

Figure 17. Energy balance of the ICE – TEG system (ICE operating condition: 6 Nm and 3800 rpm).

3.6. Energy efficiency of the ICE – TEG system

Figure 17 shows the energy balance of the ICE-TEG system for the engine operating at 6 Nm and 3600 rpm.

Results show that out of the energy output from the engine with the exhaust. The TEG recovers from 2.6 to 3.3%, which accounts for 0.64–0.81% of the energy input to the engine.

Figure 18 shows the variation of the energy efficiency of the ICE – TEG system in the range of operating variables considered.

The results show that the highest efficiency is obtained for 6 Nm at 3600 rpm, which coincides with the highest efficiency operating point of the ICE, in which the engine operates with the highest flow and energy content of the exhausts.

Table 6 compares the energy efficiency of the ICE operating with and without the TEG.

The results show that, in total, the introduction of the TEG improved the efficiency of the ICE-TEG system from a low 0.18%–0.81%. The energy of the system increases. These results highlight the need to further research the design of TEGs to upgrade the conversion efficiency of their designs.

3.7. Exergy efficiency of the ICE – TEG system

Table 7 includes the entropy generation, calculated with Eq. (6), for the operation modes of the TEG considered in the study.

Results show that the entropy generation increases with the torque in the engine. Moreover, at 3600 rpm and rotational speed, the entropy generation has a minimum, which is explained by the highest efficiency of ICE for this operating condition. Reducing the cooling water temperature reduces the entropy generation in the TEG. On average, reducing

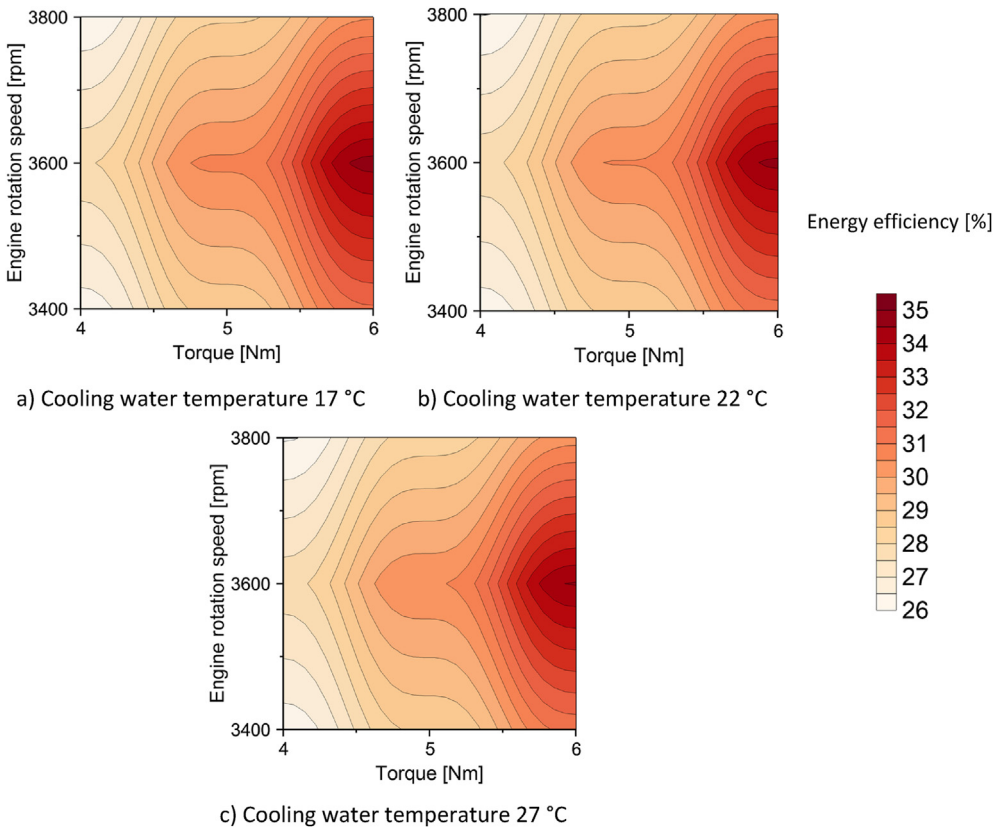

Figure 18. Variation of the energy efficiency of the ICE – TEG system.

Table 6. Energy efficiency of the ICE operating with and without the TEG.

Torque [Nm]	Rotation speed [rpm]	Energy efficiency [%]			
		Without TEG	With TEG		
			Cooling water temperature		
			17 °C	22 °C	27 °C
4	3400	26.02	26.25	26.24	26.20
	3600	27.61	27.94	27.86	27.84
	3800	25.67	26.06	25.98	25.95
5	3400	28.22	28.67	28.62	28.56
	3600	30.04	30.62	30.53	30.46
	3800	27.72	28.41	28.32	28.22
6	3400	30.62	31.42	31.26	31.15
	3600	33.91	34.71	34.63	34.54
	3800	29.63	30.44	30.36	30.28

Table 7. Entropy generation in the TEG.

Torque [Nm]	Rotation speed [rpm]	Entropy generation [W/K]		
		Cooling water temperature		
		17 °C	22 °C	27 °C
4	3400	1.151	1.154	1.162
	3600	1.190	1.205	1.210
	3800	1.155	1.171	1.178
5	3400	1.273	1.284	1.297
	3600	1.346	1.365	1.380
	3800	1.349	1.369	1.391
6	3400	1.360	1.396	1.423
	3600	1.334	1.354	1.374
	3800	1.505	1.525	1.550

the cooling temperature by 5 °C results in a reduction of 2% in the entropy generation.

Figure 19 shows the exergy balance of the ICE – TEG system.

Similarly, the results show that from the exergy output from the engine with the exhaust, the TEG recovers from 6.1% to 7.7% of the gas energy, which accounts for 0.61%–0.77% of the exergy input to the engine.

Figure 20 shows the variation of the ICE – TEG system for the range of operating conditions considered.

Similarly, the results show that the highest efficiency is obtained for 6 NM at 3600 rpm, coinciding with the highest efficiency operating point of the ICE.

Table 8 compares the exergy efficiency of the ICE operating with and without the TEG for the different operating conditions considered.

The results show that, in total, the introduction of the TEG improved the efficiency of the ICE-TEG system from0.17% to 0.76% with the proposed system.

3.8. *Influence of the TEG on the emissions of the ICE*

Since the TEG reduces the demand for fuel in ICEs, a reduction of the emissions can be expected in the engine. Figure 21 shows the emissions of CO, CO_2, NO_X, and smoke opacity in the ICE operating with and without the TEG.

Results show that the operation of the ICE with the TEG reduces the emission of pollutants in the engine. Reducing the cooling temperature reduces the emission of pollutants in the ICE, which is explained by the increased efficiency of the TEG in this case. Contrasted to the operation without TEG, the use of the TEG reduces the emissions of CO by 3.8%, 2.9%, and 1.9% cooling water temperatures of 17 °C, 22 °C, and 27 °C.

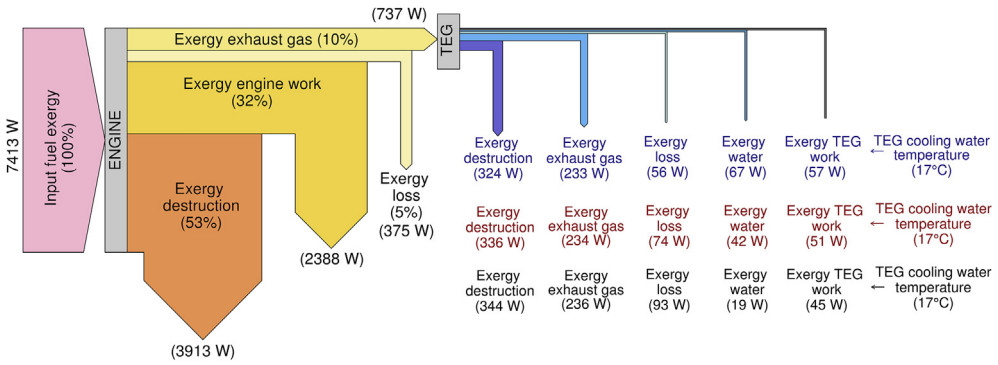

Figure 19. Exergy balance of the ICE – TEG system (ICE operating condition: 6 Nm and 3800 rpm).

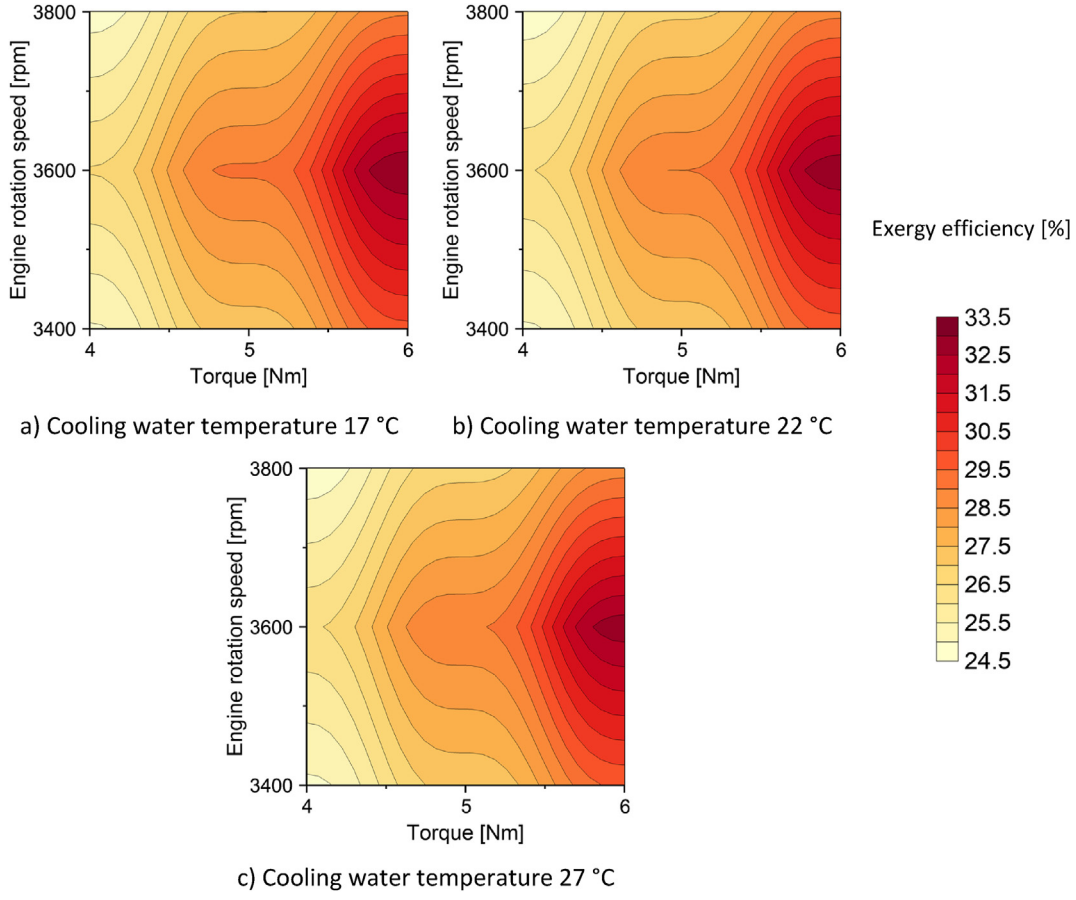

Figure 20. Variation of the exergy efficiency of the ICE – TEG system.

Similarly, the emissions of CO_2 were reduced by 3.9%, 2.9%, and 1.9%, while the emissions of NO_X were reduced by 4.3%, 3.4%, and 1.4%, and the smoke opacity was reduced by 3.9%, 2.7%, and 2.1%, respectively.

3.9. Economic analysis

An economic assessment was developed to evaluate the economic viability of the TEG discussed in this study. The assessment considers the total construction and assembly cost and the economic savings from the TEG.

The cost of the TEG is calculated using the Eq. (26).

$$C_T = C_{TEM} + C_{Exh} + C_c + C_f + C_M \tag{26}$$

where C_{TEM} is the cost of the thermoelectric modules, C_{Exh} is the cost of the heat exchanger, C_c is the cost of the rectangular ducts (see Figure 1), C_f is the total manufacturing cost and C_M is the cost of accessories/ miscellaneous.

The economic costs are provided in Table 9.

The economic savings of the TEG are associated with the reduction of fuel consumption because of the energy savings. The economic savings are calculated as [55].

$$E_{TEG} = \left(\frac{\dot{m}_{fuel}[kg/s]}{\dot{W}_{engine}[kW]} \times 3600\right) \cdot \dot{W}_{TEG}[kW] \cdot \rho_f[USD/kg] \cdot t_p \tag{27}$$

where ρ_f is the price of fuel $(1.3 USD/kg)$ and t_p is the engine operating time $(t_p = 24 hours/day)$.

Table 8. Exergy efficiency of the ICE operating with and without the TEG.

Torque [Nm]	Engine speed [rpm]	Exergy efficiency [%]			
		Without TEG	With TEG		
			Cooling water temperature		
			17 °C	22 °C	27 °C
4	3400	24.72	24.94	24.93	24.89
	3600	26.23	26.54	26.47	26.44
	3800	24.39	24.76	24.68	24.65
5	3400	26.81	27.24	27.19	27.13
	3600	28.54	29.09	29.00	28.94
	3800	26.33	26.99	26.90	26.81
6	3400	29.09	29.85	29.70	29.59
	3600	32.21	32.98	32.90	32.81
	3800	28.15	28.91	28.84	28.76

The cost of fuel is determined as [56].

$$\rho_f = \frac{1.07\ \text{USD}}{\text{litre}} \times \frac{1000\ \text{litre}}{1\ \text{m}^3} \times \frac{1\ \text{m}^3}{821.5\ \text{kg}} = 1.3 \frac{\text{USD}}{\text{kg}} \tag{28}$$

The payback duration (P_b) is calculated as [57].

$$P_b = \frac{C_{TEM} + C_{Exh} + C_c + C_f}{E_{TEG}} \tag{29}$$

Figure 22 shows the economic savings for the different water-cooling temperatures considered.

The results show that reducing the cooling temperature by 20% increases the economic savings by 11%. The savings for one year, considering the continuous use of the engine (i.e., 24 h/day), account for 86 to 107.97 USD/kW for cooling temperatures between 17% and 27 °C.

Figure 23 shows the payback period of the TEG for the different water-cooling temperatures considered.

The results show a payback period of nearly 5 years, which is similar to other TEGs reported in the literature [55, 57]. This payback period should be significantly lower for bigger engines, with higher power

Table 9. Economic costs (USD).

Type	Unitary costs	Units	Manufacturing and assembling costs	Total Costs
C_{TEM}	$ 38.5	20		$ 770
C_{Exh}	$ 154	1	$ 103	$ 257
C_c	$ 103	2	$ 103	$ 309
C_M	$ 26			$ 26
Total				**$ 1,362**

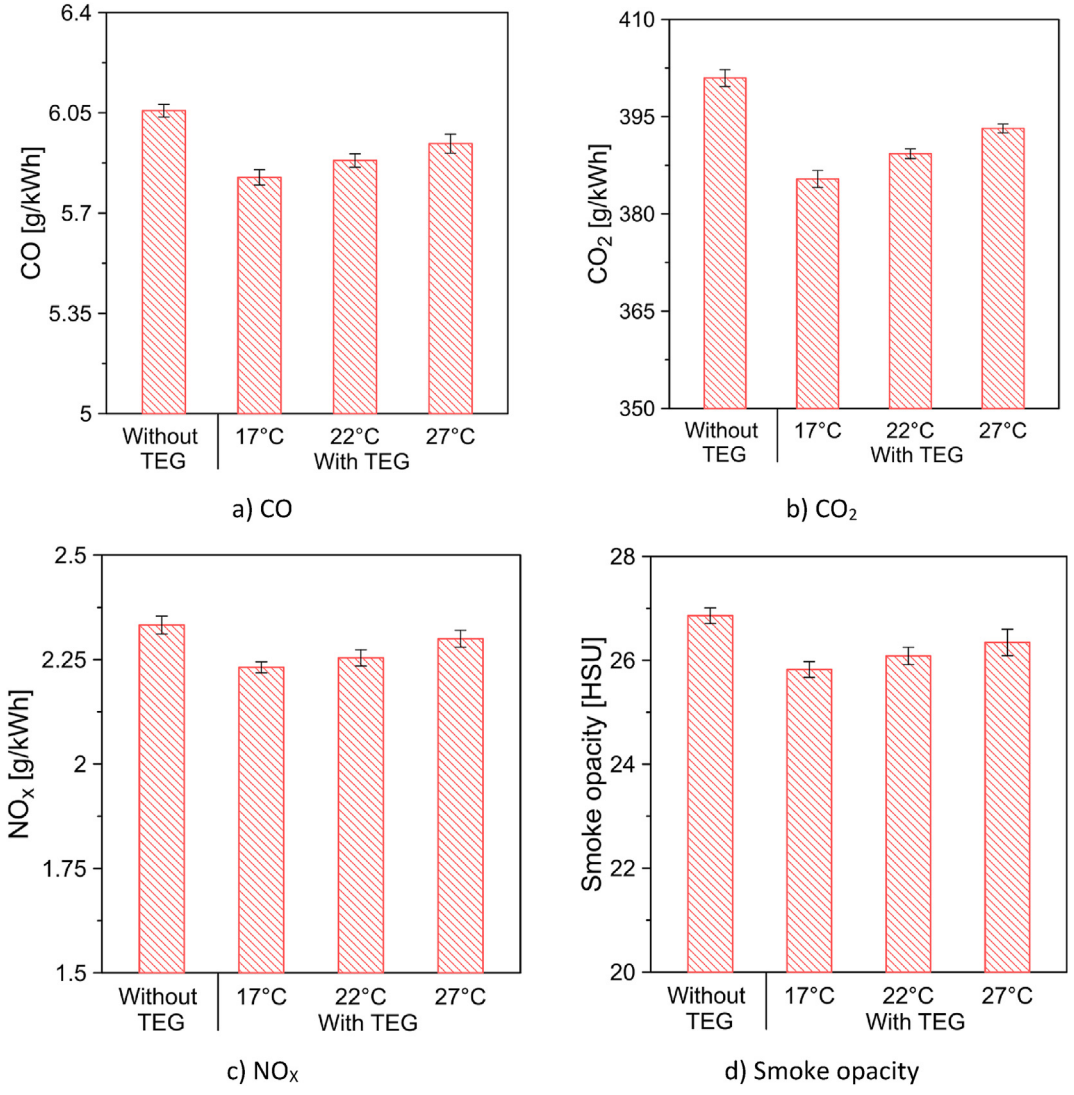

Figure 21. Emissions of the ICE operating with and without the TEG (operating condition: 6 Nm and 3800 rpm).

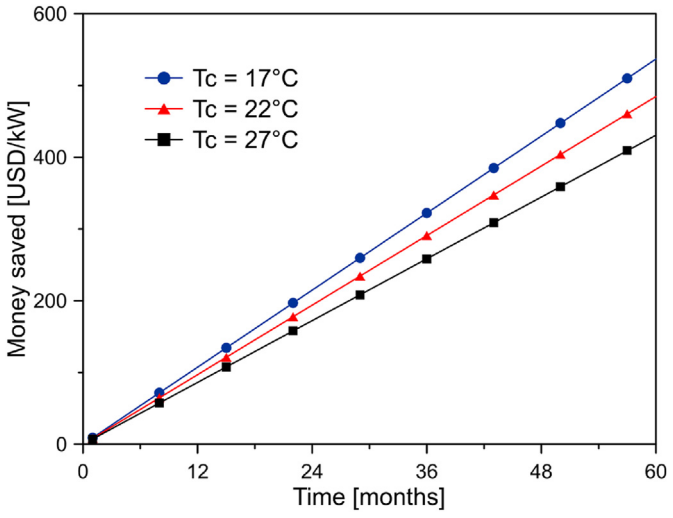

Figure 22. Economic savings resulting for the TEG (operating condition: 6 Nm and 3800 rpm).

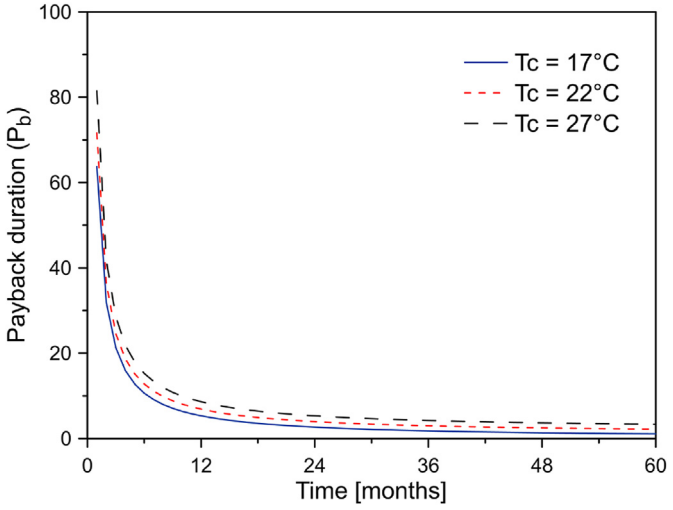

Figure 23. Payback period of the TEG (operating condition: 6 Nm and 3800 rpm).

outputs. Furthermore, in countries with high fuel costs, the payback period should be lower than the one obtained in this study.

4. Conclusions

This study introduced the analysis based on the first and second law of thermodynamics to assess the impact of the torque and rotation speed of the engine and the cooling water temperature on the performance of TEGs. The map performance of the TEG and the engine is an adequate and novel approach to highlight the characteristics of TEGs to easier identify the operating characteristics and efficiencies of these devices.

The results highlight the significance of an adequate selection of the external electric resistance based on the operating conditions of the engine, thus guaranteeing the highest energy recovery in the TEG. The incorrect definition of electric resistance can significantly affect the performance of TEGs. Moreover, the analysis shows that the engine torque has more influence on the performance of the TEG than the engine rotational speed. Particularly, the power generation was increased for the maximum torque and rotational speed of the engine. On the other hand, the cooling water temperature significantly influences the TEG performance, and on average, reducing 5 °C results in an 18% increment, upgrading the efficiency of the TEG operation. Furthermore, implementing the TEG during the operation of the ICE reduced the emissions of CO, CO_2, NO_X, and smoke opacity between 2% and 4%.

The exergy balance of the TEG shows that 31.6%–32% of the exergy is loss with the exhaust flow, while the exergy destruction accounts for 44%–47%. Therefore, there is still room to improve the performance of the TEG. Overall, a more detailed assessment is required to define the avoidable and unavoidable exergy destruction in the TEG, to define how to prevent the avoidable exergy destruction.

Overall, incorporating the TEG in ICEs stand as a significant opportunity to increase energy efficiency and reduce the emission of pollutants. Implementing a transient analysis in the TEG is an opportunity to optimize its performance, which is the subject of future studies. Other opportunities to improve efficiency include the development of advanced construction materials and more efficient cooling systems to upgrade the energy conversion in TEGs.

Declarations

Author contribution statement

Ramírez-Restrepo, R. & Duarte-Forero, J.: Conceived and designed the experiments; Performed the experiments; Analyzed and interpreted the data; Contributed reagents, materials, analysis tools or data; Wrote the paper.

Sagastume-Gutiérrez, A. & Cabello-Eras, J.: Analyzed and interpreted the data; Contributed reagents, materials, analysis tools or data; Wrote the paper.

Hernández, B.: Performed the experiments; Analyzed and interpreted the data; Wrote the paper.

Funding statement

This research did not receive any specific grant from funding agencies in the public, commercial, or not-for-profit sectors.

Data availability statement

Data included in article/supp. material/referenced in article.

Declaration of interests statement

The authors declare no conflict of interest.

Additional information

No additional information is available for this paper.

Acknowledgements

The authors thank UNIVERSIDAD DEL ATLÁNTICO, UNIVERSIDAD DE LA COSTA-CUC, and SPHERE ENERGY company for their support on the development of this research by allowing the use of their facilities and the required instrumentation.

References

[1] Y. Azoumah, J. Blin, T. Daho, Exergy efficiency applied for the performance optimization of a direct injection compression ignition (CI) engine using biofuels, Renew. Energy 34 (2009) 1494–1500.
[2] K. Eckart, P. Henshaw, Jatropha curcas L. and multifunctional platforms for the development of rural sub-Saharan Africa, Energy Sustain. Dev. 16 (2012) 303–311.
[3] S.S. Sidibé, J. Blin, G. Vaitilingom, Y. Azoumah, Use of crude filtered vegetable oil as a fuel in diesel engines state of the art: literature review, Renew. Sustain. Energy Rev. 14 (2010) 2748–2759.
[4] D. Agarwal, A.K. Agarwal, Performance and emissions characteristics of Jatropha oil (preheated and blends) in a direct injection compression ignition engine, Appl. Therm. Eng. 27 (2007) 2314–2323.

[5] G.A. Diaz, J.D. Forero, J. Garcia, A. Rincon, A. Fontalvo, A. Bula, R.V. Padilla, Maximum power from fluid flow by applying the first and second laws of thermodynamics, J. Energy Resour. Technol. 139 (2017), 032903.

[6] E. Hanff, M.-H. Dabat, J. Blin, Are biofuels an efficient technology for generating sustainable development in oil-dependent African nations? A macroeconomic assessment of the opportunities and impacts in Burkina Faso, Renew. Sustain. Energy Rev. 15 (2011) 2199–2209.

[7] G. Baquero, B. Esteban, J.-R. Riba, A. Rius, R. Puig, An evaluation of the life cycle cost of rapeseed oil as a straight vegetable oil fuel to replace petroleum diesel in agriculture, Biomass Bioenergy 35 (2011) 3687–3697.

[8] R. Escobar-Yonoff, D. Maestre-Cambronel, S. Charry, A. Rincón-Montenegro, I. Portnoy, Performance assessment and economic perspectives of integrated PEM fuel cell and PEM electrolyzer for electric power generation, Heliyon 7 (2021), e06506.

[9] F. Consuegra, A. Bula, W. Guillín, J. Sánchez, J. Duarte Forero, Instantaneous in-cylinder volume considering deformation and clearance due to lubricating film in reciprocating internal combustion engines, Energies 12 (2019) 1437.

[10] A. Ziolkowski, Automotive Thermoelectric Generator impact on the efficiency of a drive system with a combustion engine, MATEC Web Conf. 118 (2017), 00024.

[11] A. Mejía, M. Leiva, A. Rincón-Montenegro, A. Gonzalez-Quiroga, J. Duarte-Forero, Experimental assessment of emissions maps of a single-cylinder compression ignition engine powered by diesel and palm oil biodiesel-diesel fuel blends, Case Stud. Therm. Eng. 19 (2020) 100613.

[12] G. Valencia Ochoa, C. Acevedo Peñaloza, J. Duarte Forero, Combustion and performance study of low-displacement compression ignition engines operating with diesel–biodiesel blends, Appl. Sci. 10 (2020) 907.

[13] Z.-G. Shen, L.-L. Tian, X. Liu, Automotive exhaust thermoelectric generators: current status, challenges and future prospects, Energy Convers. Manag. 195 (2019) 1138–1173.

[14] J. Vazquez, M. a Sanz-Bobi, R. Palacios, A. Arenas, State of the art of thermoelectric generators based on heat recovered from the exhaust gases of automobiles, 7th Eur. Work. Thermoelectr. (2002).

[15] D. Maestre-Cambronel, J. Guzmán Barros, A. Gonzalez-Quiroga, A. Bula, J. Duarte-Forero, Thermoeconomic analysis of improved exhaust waste heat recovery system for natural gas engine based on Vortex Tube heat booster and supercritical CO2 Brayton cycle, Sustain. Energy Technol. Assessments 47 (2021) 101355.

[16] G. Von Maltitz, W. Stafford, Assessing Opportunities and Constraints for Biofuel Development in Sub-saharan Africa, CIFOR, 2011.

[17] B. Hernández-Comas, D. Maestre-Cambronel, C. Pardo-García, M.D.S. Fonseca-Vigoya, J. Pabón-León, Influence of compression rings on the dynamic characteristics and sealing capacity of the combustion chamber in diesel engines, Lubricants 9 (2021) 25–57.

[18] A. Domingues, H. Santos, M. Costa, Analysis of vehicle exhaust waste heat recovery potential using a Rankine cycle, Energy 49 (2013) 71–85.

[19] U. Larsen, T.-V. Nguyen, T. Knudsen, F. Haglind, System analysis and optimisation of a Kalina split-cycle for waste heat recovery on large marine diesel engines, Energy 64 (2014) 484–494.

[20] V. Chintala, S. Kumar, J.K. Pandey, A technical review on waste heat recovery from compression ignition engines using organic Rankine cycle, Renew. Sustain. Energy Rev. 81 (2018) 493–509.

[21] G. Valencia Ochoa, J. Piero Rojas, J. Duarte Forero, Advance exergo-economic analysis of a waste heat recovery system using ORC for a bottoming natural gas engine, Energies 13 (2020) 267.

[22] G. Valencia Ochoa, J. Cárdenas Gutierrez, J. Duarte Forero, Exergy, economic, and life-cycle assessment of ORC system for waste heat recovery in a natural gas internal combustion engine, Resources 9 (2020) 2.

[23] H. Jouhara, N. Khordehgah, S. Almahmoud, B. Delpech, A. Chauhan, S.A. Tassou, Waste heat recovery technologies and applications, Therm. Sci. Eng. Prog. 6 (2018) 268–289.

[24] S. Riffat, X. Ma, Thermoelectrics: a review of present and potential applications, Appl. Therm. Eng. 23 (2003) 913–935.

[25] R. Ramírez, A. Sagastume, J.J. Cabello, K. Valencia, B. Hernández, J. Duarte, Evaluation of the energy recovery potential of thermoelectric generators in diesel engines, J. Clean. Prod. 241 (2019) 118412–118419.

[26] R. Saidur, M. Rezaei, W.K. Muzammil, M.H. Hassan, S. Paria, M. Hasanuzzaman, Technologies to recover exhaust heat from internal combustion engines, Renew. Sustain. Energy Rev. 16 (2012) 5649–5659.

[27] T.Y. Kim, A.A. Negash, G. Cho, Experimental study of energy utilization effectiveness of thermoelectric generator on diesel engine, Energy 128 (2017) 531–539.

[28] A. Massaguer, E. Massaguer, M. Comamala, T. Pujol, L. Montoro, M.D. Cardenas, D. Carbonell, A.J. Bueno, Transient behavior under a normalized driving cycle of an automotive thermoelectric generator, Appl. Energy 206 (2017) 1282–1296.

[29] B. Li, K. Huang, Y. Yan, Y. Li, S. Twaha, J. Zhu, Heat transfer enhancement of a modularised thermoelectric power generator for passenger vehicles, Appl. Energy 205 (2017) 868–879.

[30] M. Comamala, I.R. Cózar, A. Massaguer, E. Massaguer, T. Pujol, Effects of design parameters on fuel economy and output power in an automotive thermoelectric generator, Energies 11 (2018) 3274.

[31] D. Luo, R. Wang, W. Yu, Z. Sun, X. Meng, Modelling and simulation study of a converging thermoelectric generator for engine waste heat recovery, Appl. Therm. Eng. 153 (2019) 837–847.

[32] C. Liu, Y.D. Deng, X.Y. Wang, X. Liu, Y.P. Wang, C.Q. Su, Multi-objective optimization of heat exchanger in an automotive exhaust thermoelectric generator, Appl. Therm. Eng. 108 (2016) 916–926.

[33] A. Marvão, P.J. Coelho, H.C. Rodrigues, Optimization of a thermoelectric generator for heavy-duty vehicles, Energy Convers. Manag. 179 (2019) 178–191.

[34] C. Lu, S. Wang, C. Chen, Y. Li, Effects of heat enhancement for exhaust heat exchanger on the performance of thermoelectric generator, Appl. Therm. Eng. 89 (2015) 270–279.

[35] A. Rezania, L.A. Rosendahl, S.J. Andreasen, Experimental investigation of thermoelectric power generation versus coolant pumping power in a microchannel heat sink, Int. Commun. Heat Mass Tran. 39 (2012) 1054–1058.

[36] M.A. Karri, E.F. Thacher, B.T. Helenbrook, Exhaust energy conversion by thermoelectric generator: two case studies, Energy Convers. Manag. 52 (2011) 1596–1611.

[37] D. Li, Y. Xuan, Q. Li, H. Hong, Exergy and energy analysis of photovoltaic-thermoelectric hybrid systems, Energy 126 (2017) 343–351.

[38] A. Makki, S. Omer, Y. Su, H. Sabir, Numerical investigation of heat pipe-based photovoltaic–thermoelectric generator (HP-PV/TEG) hybrid system, Energy Convers. Manag. 112 (2016) 274–287.

[39] H. Yang, G. Shu, H. Tian, X. Ma, T. Chen, P. Liu, Optimization of thermoelectric generator (TEG) integrated with three-way catalytic converter (TWC) for harvesting engine's exhaust waste heat, Appl. Therm. Eng. 144 (2018) 628–638.

[40] G. Shu, X. Ma, H. Tian, H. Yang, T. Chen, X. Li, Configuration optimization of the segmented modules in an exhaust-based thermoelectric generator for engine waste heat recovery, Energy 160 (2018) 612–624.

[41] F. Frobenius, G. Gaiser, U. Rusche, B. Weller, Thermoelectric generators for the integration into automotive exhaust systems for passenger cars and commercial vehicles, J. Electron. Mater. 45 (2016) 1433–1440.

[42] S. Lan, Z. Yang, R. Chen, R. Stobart, A dynamic model for thermoelectric generator applied to vehicle waste heat recovery, Appl. Energy 210 (2018) 327–338.

[43] F. Zhou, J. Fu, D. Li, J. Liu, C.F. Lee, Y. Yin, Experimental study on combustion, emissions and thermal balance of high compression ratio engine fueled with liquefied methane gas, Appl. Therm. Eng. 161 (2019) 114125.

[44] T.Y. Kim, J. Kwak, B. Kim, Application of compact thermoelectric generator to hybrid electric vehicle engine operating under real vehicle operating conditions, Energy Convers. Manag. 201 (2019) 112150.

[45] Y. Wang, S. Li, X. Xie, Y. Deng, X. Liu, C. Su, Performance evaluation of an automotive thermoelectric generator with inserted fins or dimpled-surface hot heat exchanger, Appl. Energy 218 (2018) 391–401.

[46] A. Montecucco, J. Siviter, A.R. Knox, The effect of temperature mismatch on thermoelectric generators electrically connected in series and parallel, Appl. Energy 123 (2014) 47–54.

[47] M.A. Rosen, Clarifying thermodynamic efficiencies and losses via exergy, Exergy, Int. J. 2 (2002) 3–5.

[48] M. Ghazikhani, M. Hatami, D.D. Ganji, M. Gorji-Bandpy, A. Behravan, G. Shahi, Exergy recovery from the exhaust cooling in a DI diesel engine for BSFC reduction purposes, Energy 65 (2014) 44–51.

[49] S. Sarıkoç, İ. Örs, S. Ünalan, An experimental study on energy-exergy analysis and sustainability index in a diesel engine with direct injection diesel-biodiesel-butanol fuel blends, Fuel 268 (2020) 117321.

[50] G. Min, D.M. Rowe, Conversion efficiency of thermoelectric combustion systems, IEEE Trans. Energy Convers. 22 (2007) 528–534.

[51] X. Niu, J. Yu, S. Wang, Experimental study on low-temperature waste heat thermoelectric generator, J. Power Sources 188 (2009) 621–626.

[52] W.-H. Chen, P.-H. Wu, X.-D. Wang, Y.-L. Lin, Power output and efficiency of a thermoelectric generator under temperature control, Energy Convers. Manag. 127 (2016) 404–415.

[53] T.Y. Kim, A. Negash, G. Cho, Experimental and numerical study of waste heat recovery characteristics of direct contact thermoelectric generator, Energy Convers. Manag. 140 (2017) 273–280.

[54] S. Nag, A. Dhar, A. Gupta, Exhaust heat recovery using thermoelectric generators: a review, in: Adv. Intern. Combust. Engine Res., Springer, 2018, pp. 193–206.

[55] C. Liu, X. Pan, X. Zheng, Y. Yan, W. Li, An experimental study of a novel prototype for two-stage thermoelectric generator from vehicle exhaust, J. Energy Inst. 89 (2016) 271–281.

[56] GlobalPetrolPrices.com, Diesel Prices, GlobalPetrolPrices.Com, 2021. https://es.globalpetrolprices.com/diesel_prices/. (Accessed 31 July 2021).

[57] D.R. Karana, R.R. Sahoo, Thermal, environmental and economic analysis of a new thermoelectric cogeneration system coupled with a diesel electricity generator, Sustain. Energy Technol. Assessments. 40 (2020) 100742.